Thermally controlled droplet formation in flow focusing geometry: Formation regimes and effect of nanoparticle suspension

Thermally controlled droplet formation in flow focusing geometry—formation regimes and effect of nanoparticle suspension

Say-Hwa Tan[1], S. M. Sohel Murshed[1], Nam-Trung Nguyen*[1], Teck Neng Wong[1] and Levent Yobas[2]

[1]School of Mechanical and Aerospace Engineering, Nanyang Technological University,
50 Nanyang Avenue, Singapore 639798, Singapore

[2]Institute of Microelectronics, Science Park II, Singapore 117685l, Singapore

*E-mail: mntnguyen@ntu.edu.sg; Tel: (+65) 6790 4457; Fax: (+65) 6792 4062

Abstract

This paper reports experimental investigations on the droplet formation of deionized water and a nanofluid in a heat-induced microfluidic flow focusing device. Besides the effect of temperature, the effects of nanoparticle suspension (nanofluid), and the flow rate of aqueous fluid on the droplet formation and size manipulation were studied. At constant flow rates of the two liquids, three different droplet breakup regimes were observed and their transition capillary numbers as well as temperatures were identified. The heat generated by an integrated microheater changes the droplet formation process. Increasing temperature enlarges the size of the droplets significantly. Present results also demonstrate that titanium oxide (15 nm)/deionized water-based nanofluid exhibits similar characteristics in droplet formation at different temperatures and any small change in the flow rate of this nanofluid has little impact on the size of the droplets formed in a flow focusing geometry.

Keywords: Microdroplets; droplet-based microfluidics; viscosity; interfacial tension; temperature

1. Introduction

In recent years, the formation and manipulation of microdroplets attract increased interest from researchers worldwide. The reasons for this interest are the potential applications of droplet-based microfluidics in various important fields such as chemical or biochemical analysis, high throughput screening, and synthesis of polymer particles [1-4]. Droplet-based microfluidic techniques are essential for large scale integration of devices for biological or chemical analyses as the microdroplets can ensure both physical and chemical isolation to its contents. Microfluidic emulsification allows the generation of microdroplets of monomer or polymeric fluids, which are subsequently solidified in-situ to form polymer colloids. The flow of two or more immiscible liquids into a microfluidic device and the formation of emulsion droplets [5-7] as well as gas bubbles [8-9] have been reported previously. T-junction [6] and flow focusing geometries [5, 8] are commonly used for droplet formation and manipulation. As flow focusing devices can produce monodisperse microdroplets or bubbles at a high frequency, several research efforts have been made on the droplet formation and manipulation through this microfluidic device. For example, droplet formation and manipulation in flow focusing devices have been achieved by various techniques such as using shear gradients [10], introducing heating effect [11], changing surfactant concentration [12], changing other parameters such as viscosity of the liquid [13], flow rate ratios and flow rates [5, 14-15]. Anna *et al* studied the formation of water droplet in a flow focusing device and showed that the droplets size can be adjusted by controlling the oil flow rate [5]. Xu and Nakajima produced highly monodisperse soybean oil droplets (<1% polydispersity) in 1 wt.% sodium dodecyl sulfate (SDS) solution by using a simple microfluidic flow focusing geometry [16]. Based on the concept of an earlier study on thermally mediated droplet breakup and switching in T-junction bifurcation [17], Nguyen *et al* demonstrated that the droplet formation in a flow focusing device can also be controlled by applying the heat at the

droplet formation location [11]. By using different flow rate ratios of two immiscible liquids, the existence of four different droplets formation regimes such as geometry-controlled or squeezing, dripping, thread formation, and jetting was found by Anna and Mayer [12]. Each regime was identified by a critical capillary number whose value changed with the concentration of surfactant added [12].

In droplet-based microfluidics, water is the most commonly used aqueous phase for generating droplets. On the other side, nanofluid is a new and innovative class of fluids, which is engineered by dispersing nanometer-sized particles in conventional fluids such as deionized water. Nanofluids were found to exhibit different thermophysical and interfacial properties such as thermal conductivity, viscosity, and surface tension as compared to their base fluids [18-22]. Nevertheless, this fluid is suitable for use in microfluidics because they contain nanoparticles, which are orders of magnitude smaller than the microfluidic devices themselves. Our group recently reported the application of nanofluids in droplet-based microfluidics for droplet formation at a T-junction microchannel [22]. Primary results showed that nanofluid can be employed as a useful aqueous phase for droplet formation and size manipulation [22]. Although the research fields of droplet-based microfluidics [4] and nanofluids [23] have attracted great interest of from both communities, no other study has been carried out on the use of nanofluids in droplet-based microfluidics.

In this paper, we investigate the formation and manipulation of droplets of deionized water and deionized water-based nanofluids in flow focusing microchannel at different temperatures. The heating effect on the droplet formation regimes at constant flow rates of both aqueous and carrier fluids is studied and the transition capillary number and temperature are identified. The effect of nanoparticle suspension and its flow rate on the droplet formation process are also investigated.

2. Experimental

2.1 Device fabrication

In this study, a microfluidic flow-focusing device (MFFD) with integrated microheater and temperature sensor were designed and fabricated. The MFFDs were fabricated using micromachining of glass and polydimethylsiloxane (PDMS) devices [11, 17]. A temperature sensor and a microheater were patterned on glass using photolithography and lift-off technique. Both microheater and temperature sensor were made of thin-film platinum. Titanium was used as the adhesion layer between glass and platinum. The microchannel network was fabricated in PDMS using soft lithography. The master mold was fabricated by photo lithography of the thick-film resist SU-8 using a transparency mask. The glass wafer with the patterned microheater and microsensor was subsequently coated with a thin PDMS layer before being bonded to the PDMS part containing the microfluidic network. This step makes sure that all channel walls have the same properties. Bonding was achieved using oxygen plasma treatment on both PDMS surfaces (Plasma-Therm Inc. Florida, USA) at 70W for 50s. The alignment was performed manually after the oxygen plasma treatment. The bonded layers were then thermally treated at 150°c for two hours to reinforce the bonding strength and ensure a leak-proof bonding interface. The heat treatment also ensured the hydrophobic recovery of the PDMS surface which was essential for the formation of water-in-oil droplets. While the microheater provides localized heating, the sensor detects the induced temperature. The footprint of the MFFD is 1cm×1cm. Figure 1 depicts the schematic concept and dimensions of the devices used in the experiment. The depth of the microchannels is 30 μm.

2.2 Experimental setup and procedure

Two precision syringe pumps (KD Scientific Inc., USA) were used to drive the oil and the aqueous fluids through the microchannels. The flow rates of both the carrier fluid and aqueous fluids were adjusted to form uniformed droplets. The temperature sensor was calibrated before the experiments so that its resistance values can be used for in-situ temperature measurement. The temperature was adjusted by changing the voltage of the heater and was monitored through the resistance of the sensor. An epi-fluorescent inverted microscope with a filter set (Nikon B-2A) was used to observe the droplets. A sensitive CMOS camera (Basler A504K, Basler AG, Germany), which has a maximum resolution of 1.3 Megapixels and a maximum frame rate of 500 fps, was employed for recording the droplet images. The recorded droplet images were then processed by a customized MATLAB program to obtain the droplet diameter. Since the measured droplet diameter is larger then channel height, the droplets have the form of a disc. Based on the recent correlation by Nie *et al* [13], the equivalent diameter of a spherical droplet with the same volume can be determined as

$$D_{eq} = 2\sqrt[3]{\frac{1}{16}[2D^3 - (D-h)^2(2D+h)]} \quad (1)$$

where h= 30 μm is the depth of the channel and D is the measured diameter of the disk. The results of the equivalent diameter are presented in this paper.

2.3 Sample materials

Sample nanofluid, which was prepared by dispersing 0.1 volume percentage of titanium dioxide (TiO_2) nanoparticles of 15 nm (spherical-shaped) in deionized water was used in this study. While mineral oil with 2% w/w Span 80 surfactant (Sigma S6760) was used as the

carrier fluid, deionized water (DIW) and nanofluids with 0.05% w/w fluorescence dye (Sigma F6377) were used as the aqueous fluids for the droplet formation.

3. Theoretical basis

In microfluidic droplet formation, the dimensionless capillary number *Ca* is the most important parameter characterizing the droplet formation through the relative importance of shear stress and interfacial tension exerted on the droplet. The capillary number is defined as [12]

$$Ca = \frac{\eta_c a G}{\gamma} \tag{2}$$

where η_c and γ are the dynamic viscosity of the carrier fluid and the interfacial tension between the carrier fluid and aqueous fluid, respectively. Furthermore, *a* is the half-width of the microchannel of the aqueous fluid, and *G* is the effective shear rate. Applying the similar approach given by Anna and Mayer [12], the shear or elongation rate for the flow focusing geometry used in this study (figure 1) can be determined from

$$G = \frac{Q_c}{h}\left[\frac{1}{wz} - \frac{1}{b^2}\right] \tag{3}$$

where Q_c is the total flow rate of carrier fluid (oil) and *h*, *b*, *w*, and z are the depth, width of the oil flow channel, width of the orifice entrance, and the distance from the end of the aqueous channel to the orifice entrance, respectively. Thus using the above shear rate given by equation (3) into equation (2), the capillary number for the present flow focusing geometry has the form

$$Ca = \frac{\eta_c a Q_c}{\gamma h}\left[\frac{1}{wz} - \frac{1}{b^2}\right] \tag{4}$$

Using the temperature dependence of viscosity, interfacial tension and the droplet size, the capillary number as a function of temperature can be determined from equation (4).

The temperature dependence interfacial tension of the aqueous fluid in oil as well as it's viscosity were previously measured by Nguyen *et al* [11]. The two empirical correlations are $\gamma = \gamma_o \exp[-0.0144(T - T_o]$ and $\eta = \eta_o \exp[-0.0344(T - T_o]$, where η_o=23.8×10^{-3} Pa·sec and γ_0=3.65×10^{-3} N/m, and T_o=25 C are the viscosity and interfacial tension at room temperature, are used to obtain the interfacial tension and viscosity at different temperatures [11]. At the room temperature (25°C), while viscosities of mineral oil with 2 w/w % surfactant (Span 80) and nanofluid are 23.8 mPa.s and 0.93 mPa.s, respectively, the interfacial tension of DIW/oil and nanofluid/oil systems are 3.65 mN/m and 15.9 mN/m, respectively. The effective viscosities of sample fluids are found to decrease significantly with increasing fluid temperature:

$$Ca(T) = \frac{\eta_0 a Q_c}{\gamma_o h}\left[\frac{1}{wz} - \frac{1}{b^2}\right]\exp(-0.02\Delta T) \qquad (5)$$

It's apparent from equation (5) that the temperature can be used to control the capillary number and consequently the formation regimes of the droplet. An increase in temperature reduces the capillary number through the influence of viscosity over interfacial tension and thus could move the formation process of the droplets across different regimes. In the past, changing formation regimes was only possible by changing the flow rate ratio or the flow rates themselves [12].

4. Results and discussion

4. 1 Thermally controlled droplet formation and regimes

In this experiment, the flow rates of the aqueous fluid (DI water) and the carrier fluid are kept constant values of 5 µl/h and 30 µl/h, respectively. At these flow rates and room temperature, a strong elongational flow of a continuous stream of the aqueous fluid flowing through a constriction draws a thin filament through the orifice. This filament subsequently breaks into droplets [12]. As the temperature at the constriction can be controlled by the microheater and the temperature sensor, the droplets are formed at different temperatures. We have observed three different droplet formation regimes in a relatively small temperature range from 25 °C to 45 °C.

At room temperature (i.e. 25°C), the droplet formation clearly followed the dripping mode as can be seen from figure 2. The characteristics of encountering this dripping regime is that the tip of the non-moving water is fixed and the oscillations are localized around the constriction. During forming a droplet, the neck, however does not block the constriction [figure 2(b)]. The breakups are observed at a fixed point at the orifice due to the focused velocity gradient created by the nozzle shape geometry [24]. As a droplet breaks free, the tip never retracts from the constriction as shown in figure 2(c)] and immediately starts forming a new droplet. In this case, the aqueous phase finger is longer and narrower. The droplet size distribution is highly monodispersed with polydispersity less than 3%. The existence of dripping regime was observed within 30°C. It also found that with an increase in temperature beyond 30°C, the droplet formation mode starts to change to another mode. As observed in this study, the possible existence of two formation regimes at a constant flow rate was previously proposed by Nguyen *et al* [11].

At a temperature of around 35°C droplet breakup was found to be geometry controlled or squeezing regime as described by Anna *et al* [5]. Figure 3 depicts the images of droplet breakup at this squeezing regime. The tip of water is some distance away upstream of the constriction. The tip gradually narrows down as it extends towards the constriction [figure

3(a)]. It then penetrates into the constriction and grows into a bulb behind the constriction until it breaks off [figure 3(b)]. The formed droplet has a diameter larger than the depth of the channel and hence assumed a disk shape. After breakup, the tip retracts back upstream as shown in figure 3(c). In order to distinguish between observed different modes of a regime, we termed this mode of squeezing as squeezing regime A.

At a temperature around 45°C, the formation changes to another mode of squeezing regime (squeezing regime B) as shown in figure 4. In the previous mode of squeezing i.e. regime A, the forming tip was pointed toward the constriction and has a relatively small radius of curvature [figure 3(c)]. Whereas in squeezing regime B, the tip grows into a bulb with a large radius of curvature before the constriction [figure 4(a)]. The bulb was then squeezed through the constriction to form the actual droplet behind the constriction, figure 4(b). After breakup, the tip retracts further upstream [figure 4(c)] as compared to the case of squeezing regime A [figure 3(c)]. This observed change of formation mode in a regime is mainly driven by effect of temperature-dependent interfacial tension at two different temperatures (i.e. 35°C and 45°C). The images shown in figures 2 and 4 clearly demonstrate that with an increase in temperature the droplet size increases significantly.

As discussed above, the capillary number represents the relative ratio of influence of the viscosity and the interfacial tension. Therefore, the capillary number (Ca) is commonly used to characterize droplet formation regime. Figure 5 depicts the capillary number as function of temperature for the liquid system and the formation processes described above. An increase in temperature results in a change in the capillary number mainly through the interfacial tension and viscosity of the carrier fluids. Figure 4 demonstrates a transformation of droplet formation regimes at constant flow rates of both fluids. For our system with an oil-DI water-oil flow rate (µl/h) ratios of 30:5:30, the first regime change was observed at 30 °C and Ca number of 0.016 (figure 5). First, the dripping regime is observed from 25 °C to

30 °C and at the capillary number range of 0.018>Ca>0.016. In the temperature range of 30 °C to 42 °C, the squeezing regime A was observed and corresponding range of the capillary number found to be 0.016>Ca>0.013. In the temperature range above 42 °C, the squeezing regime B was observed and corresponding range of the capillary number found to be Ca<0.013. The present range of capillary number for squeezing regime is within the range found by Zhou *et al* [25] from their numerical simulation. Without considering any heating effect, Zhou *et al* showed that an increase in capillary number from 0.01 (i.e. Ca>0.01) typically gives way to dripping and other subsequent regime such as jetting [25].

4.2 Effect of nanoparticle suspension

The different regimes discussed above reflect well in the measured droplet diameters. To investigate the influence of nanoparticle suspension, we compared the results of DI-water with nanofluid. To the best of our knowledge, no work has been reported on the nanofluid droplet formation in a flow focusing device. In order to explore the potential application of nanofluids in droplet-based microfluidics and to understand the effect of dispersed nanoparticles in aqueous liquid on droplet formation, a nanofluid was used for the droplet formation experiment. As can be seen from figure 6, while at 25°C the droplet sizes for DI water and nanofluid are 61.8 μm and 49.3 μm, respectively. At 45°C the droplet sizes are found to be 121.5 μm and 124.9 μm, respectively. The observed differences are mainly due to the differences in the interfacial tension and viscosity of both fluids and the dependence of temperature on these properties as reported in our previous study [22].

Both fluids exhibit similar formation behavior in three different regimes. Dripping regime, squeezing regime A, and squeezing regime B are reflected well in the change of droplet diameters, figure 6.

4.3 Effect of nanofluid flow rate

The flow rates of both aqueous and carrier fluids greatly influence the droplet formation process. Although several studies reported the effect of flow rate of carrier fluid [10, 12, 13], very few efforts are made on the effect of aqueous fluid's flow rate. Thus, the effect of different flow rates of nanofluid has been investigated in this study. As can be seen from figure 7, there is a slight decrease in droplet size with increase in water flow rate from 3 µl/h to 5 µl/h. Although this is not expected trend, at room temperature condition similar decrease was also observed by Yobas *et al* when they increased the water flow rate from 0.83 µl/min to 1.7 µl/min [26]. They however, reported only about 30% increase in droplet size due to a ten fold increase in water flow rate from 0.83 µl/min to 8.3 µl/min [26]. Our present results suggest that the droplet size is weakly dependent on the small change in the flow rate of the dispersed phase. In the case of a large change (order magnitude) of flow rate, the dependence of aqueous phase flow rate on the droplet size could be stronger.

5. Conclusions

In this study, we experimentally investigate the droplet formation and size manipulation of deionized water and deionized water-based nanofluids in heat-induced flow focusing devices. The effects of temperature, nanoparticle suspension (nanofluid), and the flow rate of nanofluid on the droplet formation are also studied.

The droplet size of both deionized water and nanofluid are found to increase with increasing the heater temperature. This demonstrates that heating with an integrated microheater at the flow focusing geometry can effectively control the droplet formation and

size manipulation. Present results also showed the dominance of viscous force over surface tension in controlling droplet physical characteristic using heat.

At constant flow rates of aqueous and carrier fluids, the droplet formation regimes can be changed by controlling the temperature. Three different flow regimes are observed and their critical capillary number and temperature were identified.

Results demonstrate that TiO_2 (15 nm)/deionized water-based nanofluid exhibit similar characteristics in droplet formation and size control with the temperature. It is also found that small change in flow rate of the aqueous phase has little impact on the size of nanofluid droplet.

Acknowledgement

The authors gratefully acknowledge the support from the Agency of Science, Technology and Research (A*STAR), Singapore (grant number SERC 052 101 0108 "Droplet-based micro/nanofluidics").

References

[1] Joanicot M, Ajdari A 2005 *Science* **309** 887-888

[2] Song H, Chen D L, Ismagilov R F 2006 *Angew. Chem. Int. Ed.* **45** 7336-7356

[3] Whitesides G M 2006 *Nature* **442** 368-373

[4] Christopher G F, Anna S L 2007 *J. Phys. D: Appl. Phys.* **40** R319-R336

[5] Anna S L, Bontoux N, Stone H A 2003 *Appl. Phys. Lett.* **82** 364-366

[6] Thorsen T, Roberts R W, Amold F H, Quake S R 2001 *Phys. Rev. Lett.* **86** 163-4166

[7] Tice J D, Song H, Lyon A D, Ismagilov R F 2003 *Langmuir* **19** 9127-9133

[8] Garstecki P, Gitlin I, Luzio W D, Whitesides G M, Kumacheva E, Stone H A 2004 *Appl. Phys. Lett.* **85** 2649-2651

[9] Cubaud T, Tatineni M, Zhong X L, Ho C M 2005 *Phys. Rev. E* **72** 37302-1–37302-4

[10] Ong W L, Hua J S, Zhang B L, Teo T Y, Zhuo J L, Nguyen N T, Ranganathan R, Yobas L 2007 *Sens. Actuat. A* **138** 203-212

[11] Nguyen N T, Ting T H, Yap Y F, Wong T N, Chai J C K, Ong W L, Zhou J L, Tan S H, Yobas L 2007 *Appl. Phys. Lett.* **91** 084102-1–084102-3

[12] Anna S L, Mayer H C 2006 *Phys. Fluids* **18** 121512-1–121512-13

[13] Nie Z, Seo M, Xu S, Lewis PC, Mok M, Kumacheva E, Whitesides G M, Garstecki P, Stone H A 2008 *Microfluid Nanofluid* 2008 (DOI 10.1007/s10404-008-0271-y)

[14] Ward T, Faivre M, Abkarian M, Stone H A 2005 *Electrophoresis* **26** 3716-3724

[15] Takeuchi S, Garstecki P, Weibel D B, Whitesides G M 2005 *Adv. Mater.* **17** 1067-1072

[16] Xu Q, Nakajima M 2004 *Appl. Phys. Lett.* **85** 3726-3728

[17] Ting T H, Yap Y F, Nguyen N T, Wong T N, Chai J C K, Yobas L 2006 *Appl. Phys. Lett.* **89** 2234101-1–234101-3

[18] Lee S, Choi S U S, Li S, Eastman J A 1999 *J. Heat Transfer* **121** 280-289

[19] Murshed S M S, Leong K C, Yang C 2005 *Int. J. Therm. Sci.* **44** 367-373

[20] Li C H, Peterson G P 2006 *Appl. Phys. Lett.* **99** 084314-1 – 084314-8

[21] Murshed S M S, Leong K C, Yang C 2008 *Int. J. Therm. Sci.* **47** 560-568

[22] Murshed S M S, Tan S H, Nguyen N T 2008 *J. Phys. D: Appl. Phys.* **41** 085502

[23] Murshed S M S, Leong K C, Yang C 2008 *Appl. Therm. Eng.* (in press, doi:10.1016/j.applthermaleng.2008.01.005)

[24] Tan Y C, Cristini V, Lee A P 2006 *Sens. Actuat. B* **114** 350-356

[25] Zhou C, Yue P, Feng J J 2006 *Phys. Fluids* **18** 092105-1–092105-14

[26] Yobas L, Martens S, Ong W L, Ranganathan R 2006 *Lab Chip* **6** 1073-1073

List of Figures

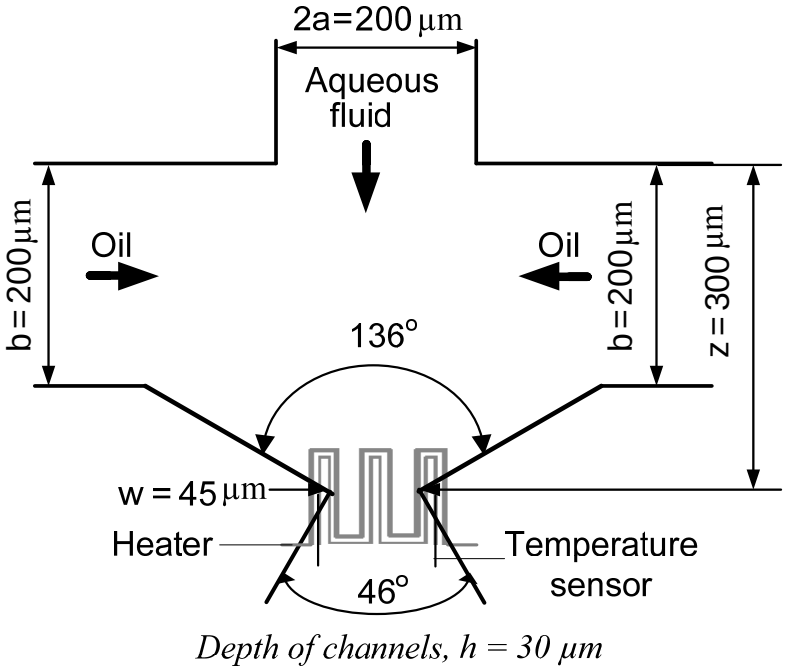

Figure 1. Schematic concept of the flow focusing devices with integrated microheater and temperature sensor for droplet formation experiments.

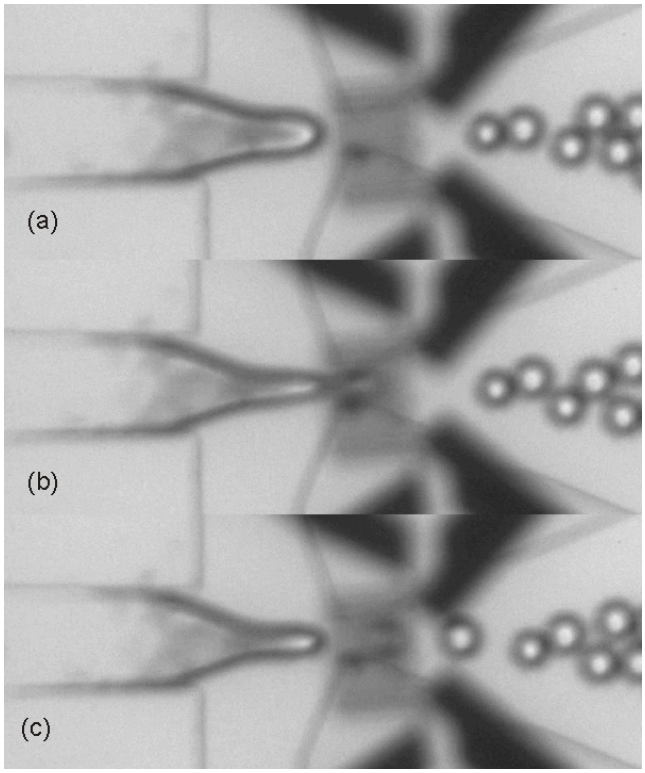

Figure 2. Dripping regime encountered at a temperature of 25°C.

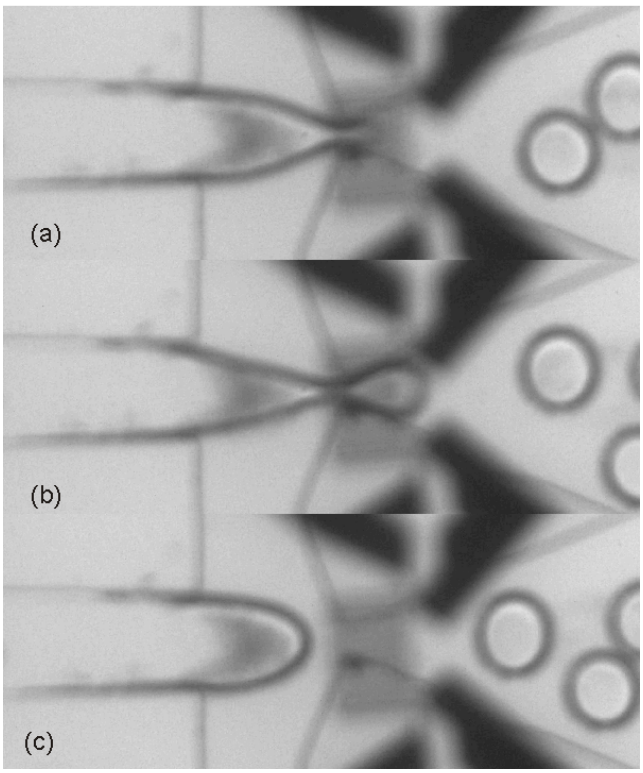

Figure 3. Squeezing regime A encountered at a temperature of 35°C.

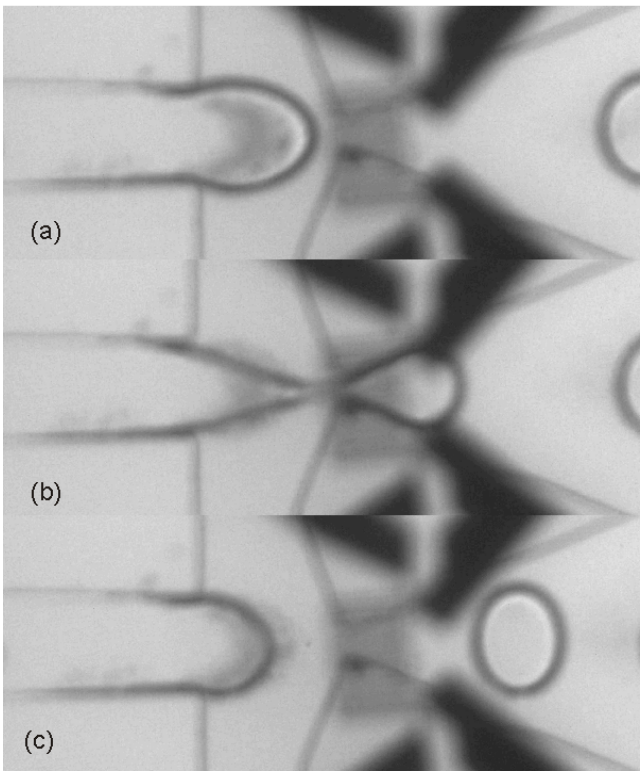

Figure 4. Squeezing regime B encountered at a temperature of 45°C.

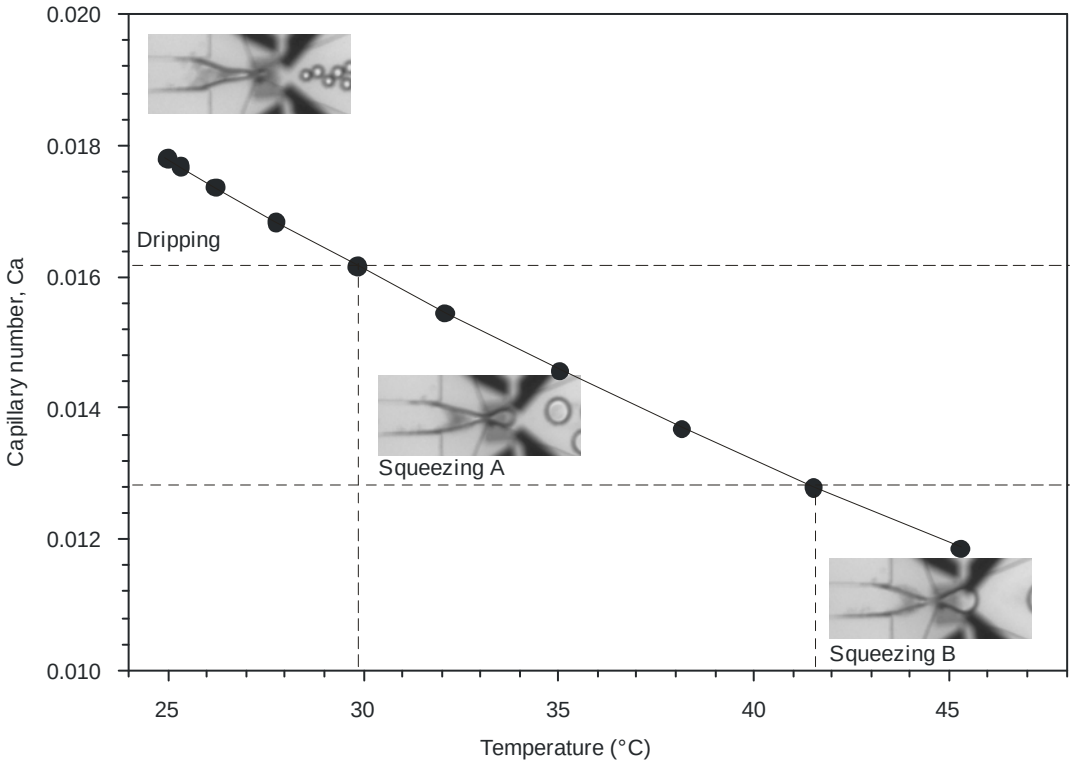

Figure 5. Capillary number and droplet formation regimes at flow rate ratio of 30:5:30 (µl/h).

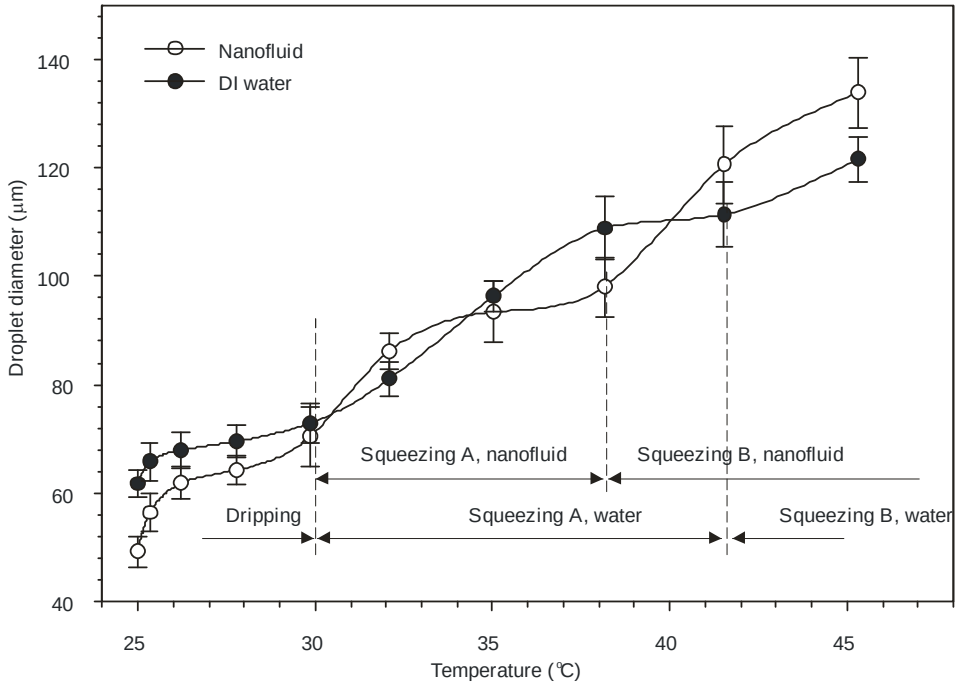

Figure 6. Comparison of droplet size of nanofluid and DI water formed at flow rate ratio of 30:5:30 (μl/h).

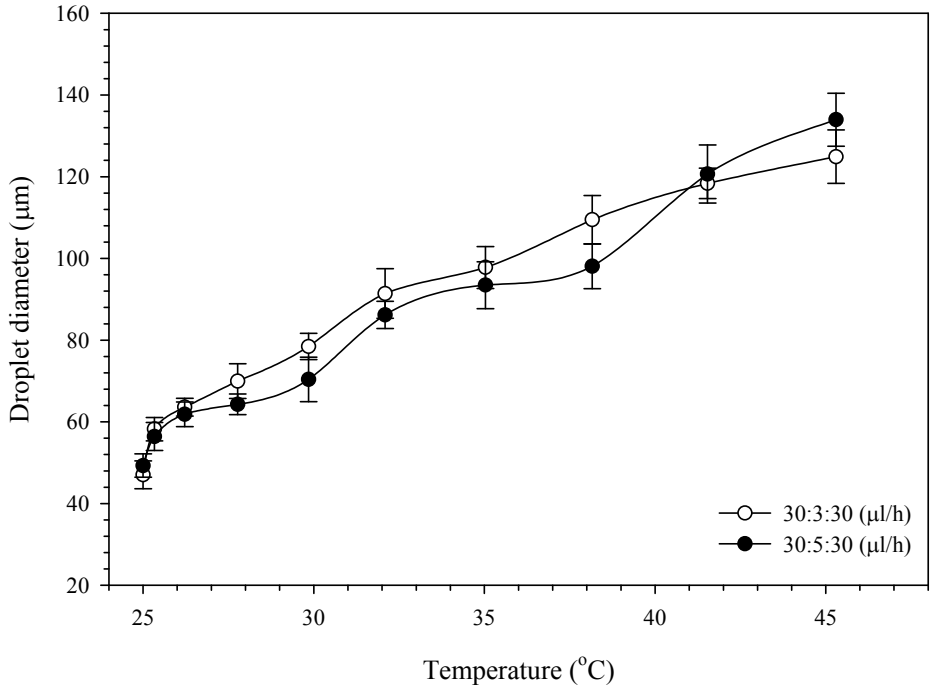

Figure 7. Effect of flow rates of nanofluid on droplet size for 30 μm channel depth.